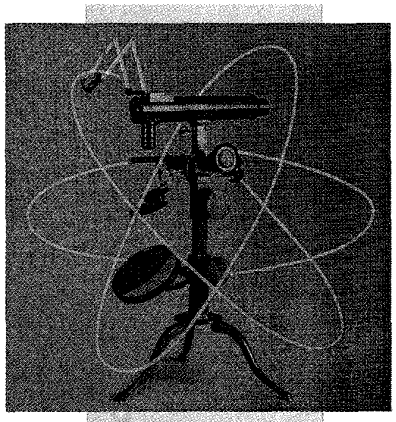

Comparing Maximum Likelihood Estimation and Constrained Tikhonov-Miller Restoration

As applied to confocal microscopy

Geert M.P. van Kempen[1], Hans T.M. van der Voort[2], Jan G.J. Bauman[3], and Karel C. Strasters[4]

[1]Pattern Recognition Group, Delft University of Technology
[2]Scientific Volume Imaging B.V.
[3]E.C. Slater Institute, University of Amsterdam
[4]Philips Medical Systems, Best, The Netherlands

The main contribution of the confocal microscope to microscopy is that it provides a practical method to obtain microscopic volume images. Although a confocal microscope is a true volume imager, its imaging properties give rise to a blurring phenomenon similar to the one in a conventional microscope, but with a reduced range [1]. The resulting distortions hamper subsequent quantitative analysis. Therefore, operations that invert the distortions of the microscope may improve these analyses. In previous work[2], the iterative constrained Tikhonov-Miller (ICTM) inversion was used to restore diffraction-induced distortions. Quantitative texture measurements, based on the grey value distance transform, showed that the results improved when applied to images after restoration.

The use of the ICTM restoration method was motivated by the linear system model used to describe the imaging properties of a confocal microscope. In this model, the image is a convolution of the object function with the point spread function of the microscope and distorted by additive noise.

This image formation model breaks down on images with a low signal-to-noise ratio, where the additive noise model is a poor description of the actual photon-limited image recording. Under these circumstances, the noise characteristics are best described by a Poisson point process, which motivates the use of restoration methods optimized for Poisson- noise distorted images.

In this article, we compare the expectation-maximization (EM) algorithm for computing the maximum likelihood estimator (MLE) for the intensity of a Poisson process, with the ICTM inversion.

A growing amount of literature is being published on the restoration of microscope images, using restoration methods such as EM-MLE [3,4] and ICTM [1,5]. Whereas these methods have just come within reach in terms of computational complexity, they have been shown to improve significantly the (quantitative) analysis of microscope images [3]. Due their non-linear nature, these methods are capable of restoring data from missing frequencies, as induced by the missing cone of the 3D OTF of incoherent light microscopes [4,6,7]. Therefore, they significantly reduce the diffraction-induced distortion found in confocal and conventional 3D images [4,7]. Finally, point spread function (PSF) measurements on optimized microscopes (such as 4π microscope and the two-photon microscope) show that images recorded by them need to be restored to reduce PSF induced artifacts before they can be analyzed [8].

Image Restoration Methods

The aim of the image restoration discussed in this section is to correct image distortions caused by the diffraction in a confocal fluorescence microscope. The incoherent nature of the emitted fluorescence light allows us to model the image formation of the confocal fluorescence microscope (CFM) as a convolution of the object function $f(x)$ with the point spread function $h(\mathbf{y}\text{-}\mathbf{x})$ of the microscope, with $\mathbf{x}$ being a 3D coordinate vector in the object space X, and $\mathbf{y}$ in the image space Y. The image $g(y)$ formed by an ideal noise free CFM can thus be written as:

$$g(y) = \int_x h(y-x) f(x) dx \quad (1)$$

Due to the photon nature of light and its effect on $f(x)$, $g(y)$ is distorted by noise. Noise, caused by photon-counting (Poisson noise), by the readout of the detector (Gaussian), and by the analog-to-digital conversion (uniform), disturbs the image. We model this noise distortion here in a general way:

$$m(y) = N(g(y)) \quad (2)$$

with $m(y)$ being the recorded image and $N()$ the noise distortion function. (In the case of additive noise, $N(x)$ equals $x+n$, with n the additive noise.)

Restoration methods are based on finding an approximate solution, $\hat{f}$, from a set of feasible solutions, according to certain criteria. These criteria depend on the type of noise, imposed regularization, and constraints set on the solutions found by the restoration algorithm. Although both the EM-MLE algorithm and the ICTM inversion are in principle based on maximum likelihood estimation, they differ significantly due to the different modeling of noise distortion on the image and the imposed constraints and regularization.

The EM-MLE algorithm computes the maximum likelihood estimator for estimating the intensity of a Poisson process. In the case where the noise distortion is additive Gaussian noise, the maximum likelihood criterion results in a mean-square-error criterion. The ICTM inversion is a constrained, regularized mean-square-error restoration method for finding a non-negative solution for images disturbed by additive noise.

Maximum Likelihood Estimation using the Expectation-Maximization Algorithm

A confocal microscope acquires an image of an object by scanning the object in three dimensions. At each point of the image, the emitted fluorescence light from the object is focused on the detector. (This light is converted by a photomultiplier tube into an electrical signal, and represented by a discrete value after an 8-bit A/D conversion.) Under low light-level conditions, the detector behaves essentially as a photon counter. This conversion of fluorescence intensity to a descrete number of detected photons is described statistically as a Poisson process. The log likelihood function of Eq. 2, for $N()$ being a Poisson point process, is given by[9]:

$$L(\hat{f}) = -\int_Y \hat{g}(y) dy + \int_Y \ln[\hat{g}(y)] m(y) dy \quad (3)$$

with:

$$\hat{g}(y) = \int_X h(y-x) \hat{f}(x) dx$$

The maximum likelihood solution for $\hat{f}$ of Eq. 3 is:

$$\hat{f}_{MLE} = \max L(\hat{f}; m, h) \quad (4)$$

which can be found using the EM algorithm, as described by Dempster, Laird and Rubin [10]. This iterative algorithm was used first by Shepp and Vardi [11] for computing the MLE of the intensity of a Poisson point process. The EM-MLE solution for Eq. 4 is:

$$\hat{f}^{k+1}(x) = \hat{f}^k(x) \int_y \left[\frac{h(x-y)}{\int_x h(y-x) \hat{f}^k(x) dx} \right] m(y) dy \quad (5)$$

The EM-MLE algorithm insures a non-negative solution when an non-negative initial guess $\hat{f}$ is used. Furthermore, Vardi, et al.,[12] have shown that the likelihood of each iteration of the EM-MLE algorithm will strictly increase to a global maximum.

The EM-MLE method for estimating the intensity of a Poisson point process is identical to the restoration algorithm that Richardson and Lucy [13] derived using different arguments.

In fluorescence microscopy, it is common to measure a non-zero background level arising from auto-fluorescence, inadequate removal of fluorescent staining material, or electronic sources. When this background signal is modeled as a spatial invariant Poisson point processes, the EM-MLE estimator results in [2]:

$$\hat{f}^{k+1}(x) = \hat{f}^k(x) \int_y \left[\frac{h(x-y)}{\int_x (h(y-x) \hat{f}^k(x) + b) dx} \right] m(y) dy \quad (6)$$

with b the average background intensity.

Iterative Constrained Tikhonov-Miller Inversion

In this section, we closely follow the derivation of ICTM inversion as given by Van der Voort and Strasters [1]. The inversion is based on the assumption that the general noise distortion function (Eq. 2) can be modeled as an additive noise function [14]:

$$m(y) = g(y) + n \quad (7)$$

For images with a relative high signal-to-noise ratio, the additive noise model can be motivated by the central limit theorem [9]: Under these circumstances, the distribution of a Poisson process can be approximated with a Gaussian distribution.

The Tikhonov-Miller (TM) inversion combines two selection criteria for finding $\hat{f}$ in one quadratic functional:

$$\Phi(\hat{f}) = \left\| g - h \otimes \hat{f} \right\|^2 + \left(\frac{\varepsilon}{E} \right)^2 \left\| r \otimes \hat{f} \right\|^2 \quad (8)$$

with ε an estimate of the norm of the noise, E the power of the object, r a regularization operator, and $\otimes$ the convolution operator. The $\|.\|$ norm is defined by:

$$\|f\|^2 = \int_x |f(x)|^2 dx \quad (9)$$

The TM functional consists of a mean-square-error criterion and a stabilizing function, constrained by an energy bound. This regularizing functional suppresses solutions of $\hat{f}$ that oscillate wildly due to spectral components outside the bandwidth of h. Minimization of Eq. 8 yields the well-known TM solution:

$$\hat{F} = \frac{H^* G}{\|H\|^2 + \eta \|C\|^2} \quad (10)$$

with $\eta = (\varepsilon/E)^2$, * denoting the conjugate operator, and capital letters the Fourier transform of the corresponding function. Although this solution requires modest computational efforts, it is very sensitive to errors in the estimation of the PSF, causing ringing artifacts [1]. Furthermore, the TM inversion is a linear solution, thus not capable of restoring missing spatial frequency components. Finally, the solution may contain negative values. This latter property of the TM inversion is a major drawback, since the intensity of an object is imaged, which is always positive.

A solution to these disadvantages of the TM solution is to solve Eq. 8 with an iterative procedure, the ICTM method. Such a procedure can constrain the solution $\hat{f}$ to be non-negative, by clipping each successive estimate.

We used the method of conjugate gradients to implement the TM inversion in an iterative way[14]. This is a modification to the steepest descent method, which gives faster convergence[14] in the case

of a quadratic functional. The so-called conjugate direction is given by:

$$p_k = r_k + \gamma_k p_{k-1} \tag{11}$$

with:

$$\gamma_k = \frac{\|r_k\|}{\|r_{k-1}\|}$$

and r_k denoting the steepest descent direction:

$$r_k = -\frac{1}{2}\nabla_f \Phi(\hat{f}) = (\|h\| + \eta)\hat{f}_k + h^* \otimes g \tag{12}$$

A new conjugate gradient estimate is now found as:

$$\hat{f}_{k+1} = \hat{f}_k + \beta p_k \tag{13}$$

In absence of a non-linear constraint, the step size, β, can be calculated analytically. However, in the presence of such a constraint, the optimal β must be searched for iteratively. In our implementation, a golden section rule line-search algorithm [15] is employed to find β. Thus, the algorithm consists of a main iterative loop in which the conjugate directions are computed, and a subiterative loop in which β is optimized and the new estimate of $\hat{f}$ is found.

Stopping Criteria

In principle, one can continue to generate new estimates of $\hat{f}$ until the solution is optimal with respect to the functional of the applied restoration method (log-likelihood for EM-MLE, Eq. (8) for ICTM). In practice, this procedure is undesirable. Experiments[16] show that the likelihood of an EM-MLE estimate increases logarithmic as a function of the number of iterations. This growth makes the search for the maximum of the likelihood function extremely computational expensive. Furthermore, Lagendijk [14] shows that noise amplifications can seriously deteriorate the ICTM result when it is pursued for a large number of iterations. We have therefore used a threshold (typically 0.001%) on the change of the functional

$$(\hat{f}_{k+1} - \hat{f}_k) / \hat{f}_k$$

to stop the iterations.

Implementation Considerations

Both restoration methods impose a relative large computation burden. As can be seen from Eq 5, the EM-MLE algorithm requires two convolutions for each iteration. For efficiency, these iterations are evaluated in the Fourier domain. However, the multiplication and division can best be performed in the spatial domain, requiring an additional inverse transformation, resulting in three Fourier transforms for each iteration. The subiterative loop to estimate β imposes the largest computational burden for ICTM algorithm. Although this loop is implemented with only one Fourier transform per iteration, it still has large computational complexity.

In our simulations, we have used a symmetrical PSF, allowing the use of the fast Hartley transform (FHT) [17] to calculate the convolutions. In the FHT, the multiplication of complex numbers is replaced by multiplication of real numbers, reducing the number of floating point operations by a factor of four, and the amount of memory required by two.

Experiments and Results

In this section, we describe the implementation and results of three simulation experiments. In a first experiment, we compared the results of EM-MLE and ICTM algorithms on spheres convolved with a confocal point spread function (CPSF). We compared the restoration results using the mean-square-error and I-Divergence distance measures. These measures were chosen because the restoration methods investigated minimize these distances.

In a second experiment, we investigated the influence of the restoration methods on the measurement of the CPSF as was done by Van der Voort and Strasters [2]. We used their approach, and compare the ICTM results with EM-MLE.

In a third experiment, the influence of EM-MLE and ICTM on quantitative texture analysis of confocal images was investigated. The restoration methods were used prior to a quantitative texture measure based on the grey value distance transform (GDT). Finally, the restoration of a confocal image with EM-MLE and ICTM was performed.

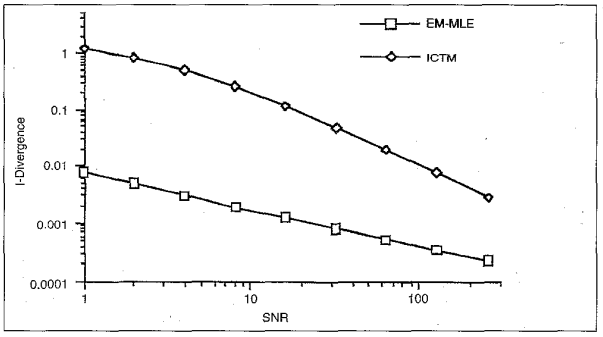

1. The I-Divergence of the EM-MLE and ICTM restoration of spheres as a function of the signal-to-noise ratio.

Restoration of Spheres

In this experiment we compare the performances of the EM-MLE and ICTM algorithms on the restoration of spheres convolved with a CPSF and distorted by Poisson noise. The spheres were generated using an analytical description of their Fourier transform, as given by[18] in spherical coordinates:

$$S_{sphere}\left(\frac{f}{r},0,0\right) = \frac{-6\pi\cos(2\pi f) + 3\sin(2\pi f)}{4\pi^3 f^3} \tag{14}$$

with r the radius of the sphere. The Fourier transform is multiplied by the confocal OTF to ensure bandlimitation. Generated in this way, the spheres are free from aliasing effects, which arise from sampling non-bandlimited analytical objects.

We computed the point spread function from a theoretical model of the CPSF, based on electromagnetic diffraction theory [2]. This model takes important microscopic parameters, such as the finite size pinhole, high apertures and polarization effects into account; lens aberrations are not modeled.

The performance of the restoration algorithms is measured as function of the signal-to-noise ratio (SNR), as defined by:

$$SNR = \frac{E}{\varepsilon} \tag{15}$$

The simulated images are distorted by Poisson noise. The noise is generated by using the intensity of the convolved spheres as averages of spatial variant Poisson point processes [15]. We have varied the SNR ratio of the simulated images by changing the photon-conversion efficiency. For Poisson processes, the variance equals the mean, so the noise power in the image is given by:

$$\varepsilon = \sigma^2 = c\tfrac{4}{3}\pi r^3 I_0 + cVI_b \tag{16}$$

with c the photon-conversion efficiency, V the image volume, I_o the average object intensity and I_b of the background. Using Eqs. 15 and 16, the photon-conversion can now be found with:

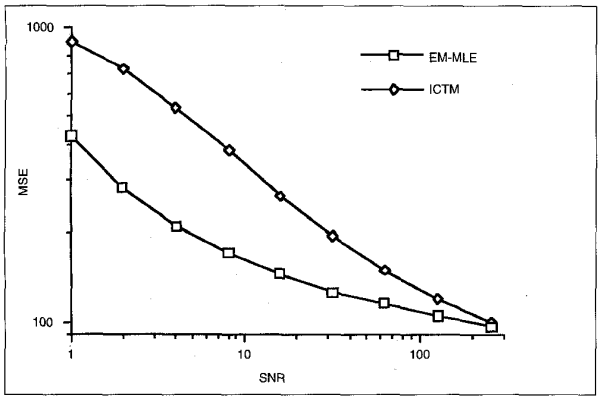

2. The MSE of the EM-MLE and ICTM restoration of spheres as a function of the signal-to-noise ratio.

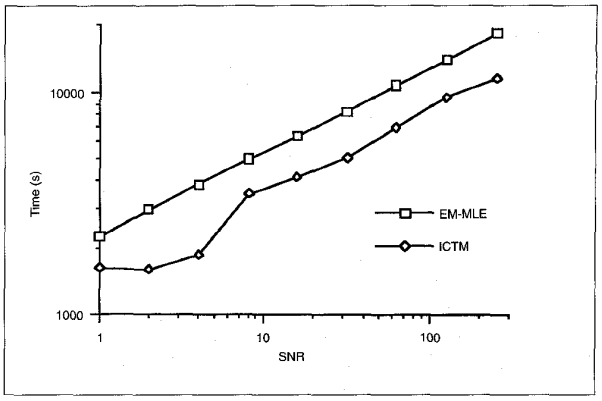

3. The processing time (in seconds) of the EM-MLE and ICTM restoration of spheres as a function of the signal-to-noise ratio. The image size was 128x128x64 floating point voxels. The times were measured on a SGI Indigo (R4400 CPU at 150 Mhz with 128 MB memory).

$$c = \frac{\frac{4}{3}\pi r^3 I_0^2}{SNR \cdot \left(\frac{4}{3}\pi r^3 I_0 + V I_b\right)} \quad (17)$$

The images were generated with a sampling density of twice the Nyquist frequency. An important motivation for this choice is given by the multiplicative iterative updating of the EM-MLE algorithm (Eq. 5). The spatial multiplication of $\hat{f}$ results in a convolution of $\hat{f}$ in the Fourier domain, giving rise to potential aliasing effects. By sampling at significantly higher frequency than the Nyquist frequency, these aliasing effects are reduced.

A second reason for choosing this high sampling density is that the signal-to-noise measurement method of Van der Voort and Strasters [2] can be used to measure the SNR of confocal images. This methods fits a spectral model of the noise in the part of the spectrum above Nyquist and extrapolates this in the lower part of the spectrum to give an estimate of the noise energy. The object energy is equal to the difference of the total spectrum and the estimated noise spectrum.

For our simulations, we have selected microscopic parameters corresponding to typical working conditions: a numerical aperture of 1.3, a refractive index of the lensoil of 1.515, an excitation wave length of 479 nm, an excitation/emission ratio of 0.9, and a pinhole size of 282 nm. These conditions resulted in a lateral sampling distance of 23.0 nm and an axial sampling distance of 81.2 nm. The images are 128 x 128 x 64 pixels in size, the spheres have a radius of 690.0 nm. The SNR ranges from 1.0 to 256.0 (0.0 dB to 24.2 dB).

Performance Measures

The performance of the EM-MLE and ICTM algorithms are measured using the mean square error (MSE) and the I-Divergence measure. The MSE is given as:

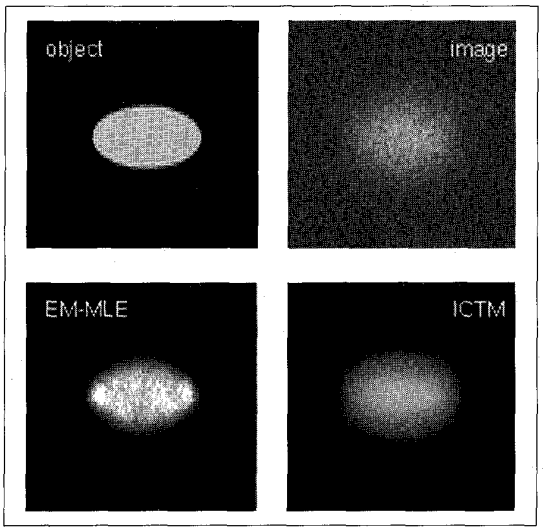

4. Restoration of spheres, the object (top-left), the confocal image of the object with a SNR of 16.0 (top-right), the restoration result with EM-MLE (bottom-left) and ICTM (bottom-right). The image size is 128x128x64 voxels, with a voxel size of 23.0x23.0x81.4 nm. The object intensity is 200.0, with a background of 40.0, with a photon-conversion of 0.58.

$$MSE\left(\hat{f}, f\right) = \left\| f - \hat{f} \right\|^2 \quad (18)$$

Csiszár[19] has introduced the I-Divergence:

$$I(a\|b) = a \ln\left[\frac{a}{b}\right] - (a - b) \quad (19)$$

to measure the distance of a function b to a function a. He has postulated a set of axioms of regularity (consistency, distinctness, and continuity) and locality that a distance measure should posses. He concluded that for functions which are required to be non-negative, the I-Divergence is the only consistent distance measure. For real-valued functions having both negative and positive values, the MSE is the only consistent choice.

Snyder, et al., [20] have shown that maximizing the mean of the log-likelihood of Eq. 3 is equal to minimizing Csiszár's I-Divergence:

$$I(f\|\hat{f}) = L(f) - E\left[L(\hat{f})\right]$$

$$= \int_Y \left(\left(g(y) \ln\left[\frac{g(y)}{\hat{g}(y)}\right] - g(y) + \hat{g}(y) \right) dy \right) \quad (20)$$

with $E[\,]$ the expectation operator.

Restoration Results

Figures 1 and 2 show the I-Divergence and MSE performance of the EM-MLE and ICTM methods on the restoration of spheres, as a function of the SNR ratio. The I-Divergence and the MSE

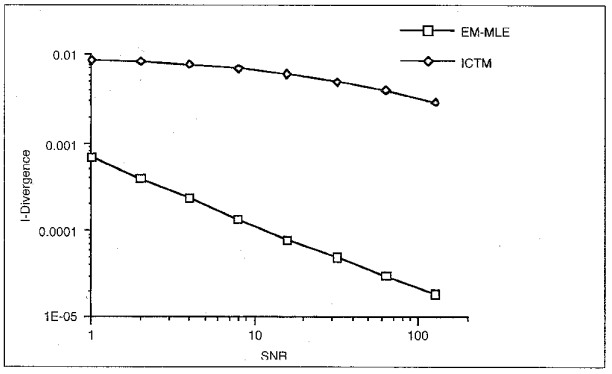

5. The I-Divergence of the EM-MLE and ICTM result of the restoration of the PSF as a function of the signal-to-noise ratio.

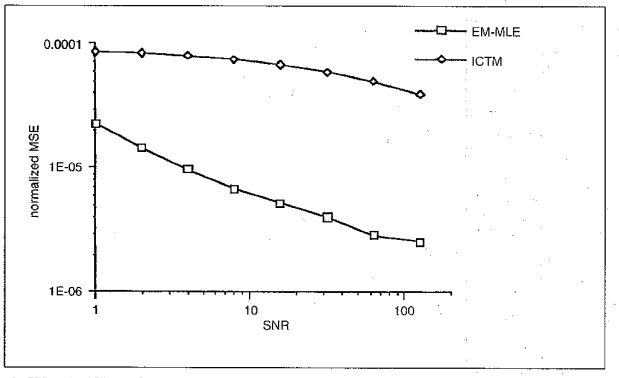

6. The MSE of the EM-MLE and ICTM result of the restoration of the PSF as a function of the signal-to-noise ratio. The MSE values are normalized by dividing them with the squared maximum value of the PSF.

performance of EM-MLE is in most cases an order of magnitude better than of ICTM. Only for a high SNR, the MSE performance of ICTM approaches the EM-MLE. The processing time of the two algorithms, as shown in Fig. 3, is measured on a SGI Indigo computer with an R4400 CPU running at 150 MHz, with 128 MB memory (Silicon Graphics, Mountain View, CA). The time of the ICTM is about 65% of the EM-MLE time. The processing times of both algorithms increase strongly as a function of the SNR. An example of the restoration with EM-MLE and ICTM is shown in Fig. 4, together with the object and its confocal image.

Measurements of the Point Spread Function

In this experiment, we investigated the influence of the restoration algorithms on the measurement method of the CPSF, as described by Van der Voort and Strasters[2]. A CPSF can, in principle, be obtained by imaging a point-like object. However, due to bleaching effects, recording images of such objects with a sufficient SNR is not feasible.

However, since the PSF is the *image* of a point object, it is non-negative, therefore the role of the object function and PSF in the ICTM algorithm can be completely reversed. As can be seen from Eq. 5, the same argument holds for the EM-MLE algorithm.

Van der Voort and Strasters [2] recorded fluorescent latex spheres (230 nm surface-stained "microbrite" spheres, Polysciences) and after a subpixel alignment of their centers of mass, averaged 32 to obtain images with a sufficient SNR. By using the analytical description of band-

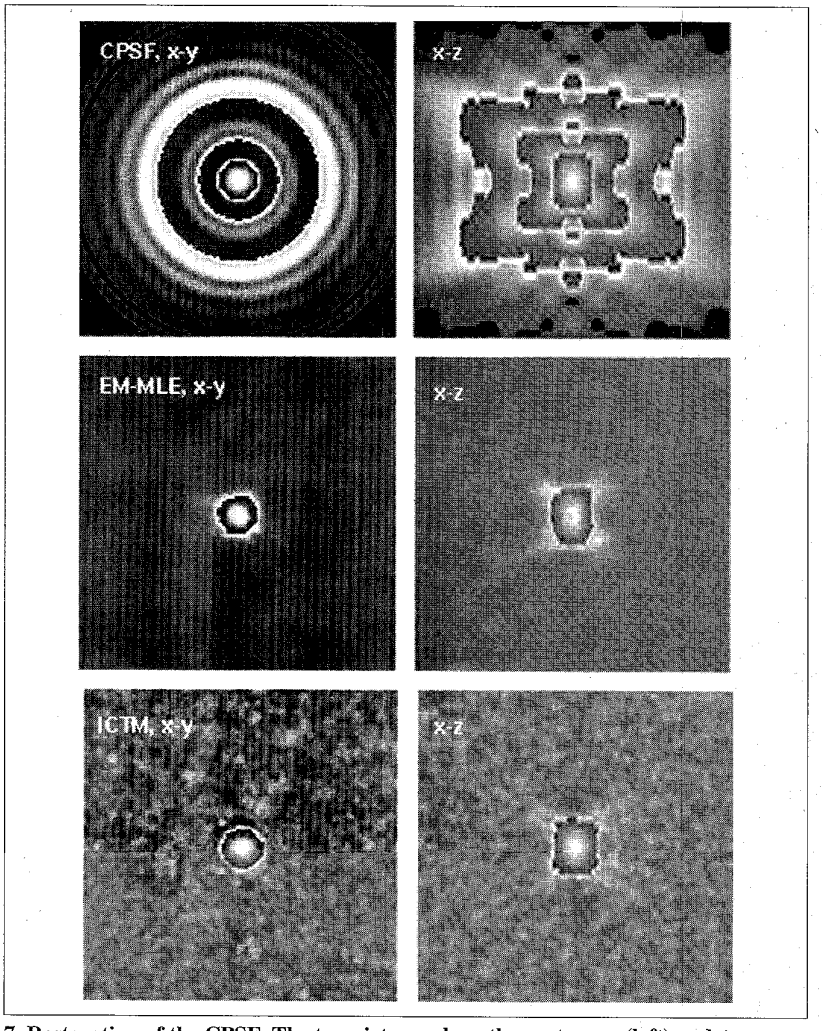

7. Restoration of the CPSF. The top pictures show the center x-y (left) and x-z (right) planes of the theoretical PSF of a confocal microscope. The middle two pictures show EM-MLE restoration of the PSF convolved with a 230.0 nm sphere (SNR of 16.0). The bottom pictures show the center x-y (left) and x-z (right) planes of the ICTM restoration result. Each transition from black to white represent an intensity reduction of a factor of ten relative to the maximum image intensity.

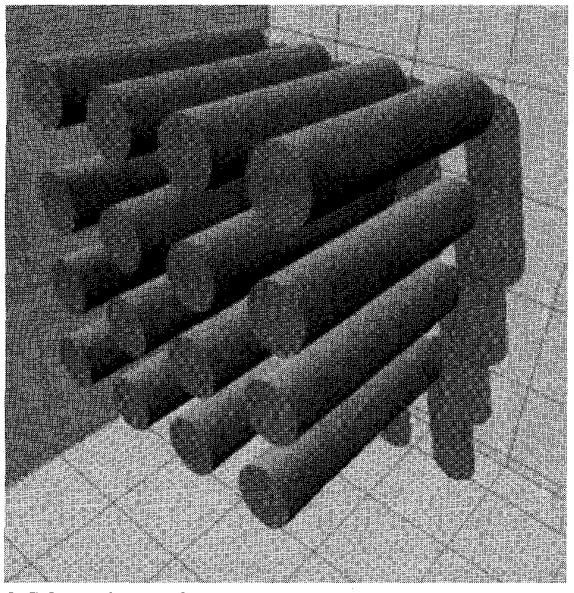

8. Schematic model of the multiple cylindrical objects as used in figures 9, 10 and 11.

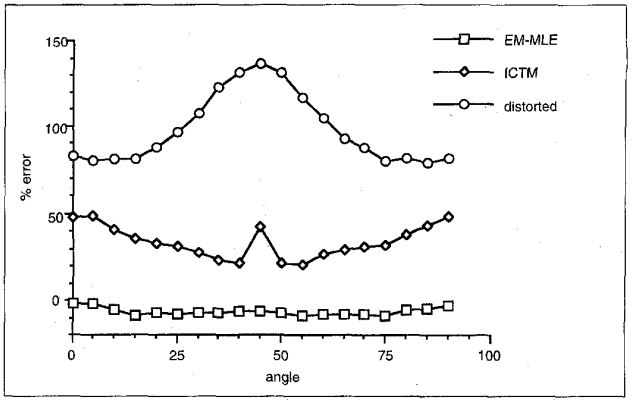

9. Error in the GDT texture measure due to diffraction-induced distortions before and after restoration with EM-MLE and ICTM. Horizontal axis: rotation angle of the object with respect to the focal plane. Vertical axis: percentage of the relative error between the texture measure derived from the image and the texture measure of the synthetic object.

limited spheres (Eq. 14), a restoration algorithm can be used to correct for the non-flat object spectrum, and thus restore the PSF image. We compare the ICTM inversion results of Van der Voort and Strasters [2] with EM-MLE restoration for obtaining the PSF images.

For the simulations, we have generated the images in the same way as described above. The diameter of the generated spheres is 230 nm, and the restoration results are again compared as a function of the SNR. Figures 5 and 6 show the I-Divergence and MSE performance measures of both methods, as a function of the SNR. The generated PSFs are normalized in such a way that the sum of the intensities of all pixels equals one. This results in very small pixel intensities, and thus very small MSE values. We have chosen to divide the MSE values of Fig. 6 by the maximum pixel intensity squared found in the original PSF image. The MSE values can now be interpreted as an average intensity difference relative to the maximum pixel intensity of the generated PSF. Figure 7 shows the center x-y and x-z planes of the

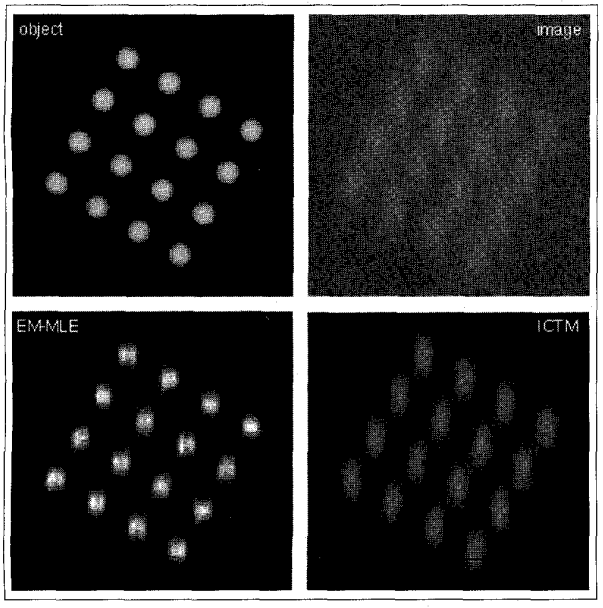

10. The EM-MLE and ICTM restoration result of the multiple cylindrical objects, with the object (top-left), its confocal image (top-right), the EM-MLE result (bottom-left) and the ICTM result (bottom-right).

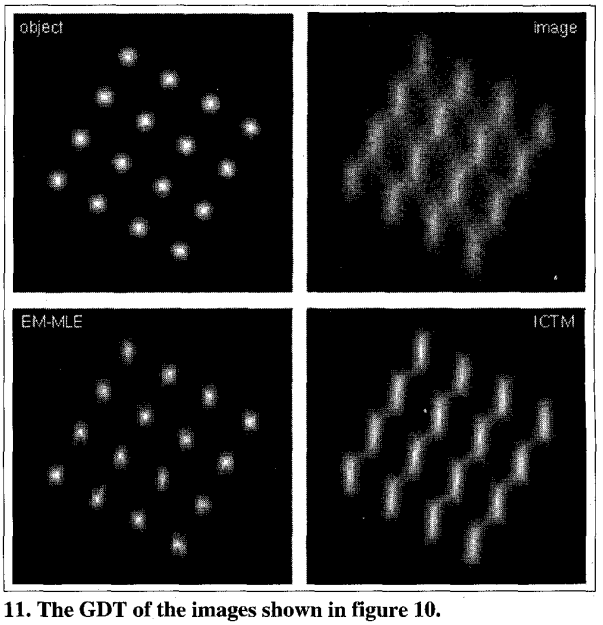

11. The GDT of the images shown in figure 10.

original PSF and the restoration results of EM-MLE and ICTM for a SNR of 16.0.

Improvement of GDT Based Texture Analysis

Van der Voort and Strasters[2] investigated the effect of restoration on texture analysis. Synthetic cylinder images were distorted with a theoretical CPSF and these images were then restored using the ICTM inversion. The texture measure, based on the GDT, measures the inaccessibility of an object. The blurring of an object with a CPSF greatly increases its inaccessibility. It was shown that the ICTM restoration significantly reduces the inaccessible area.

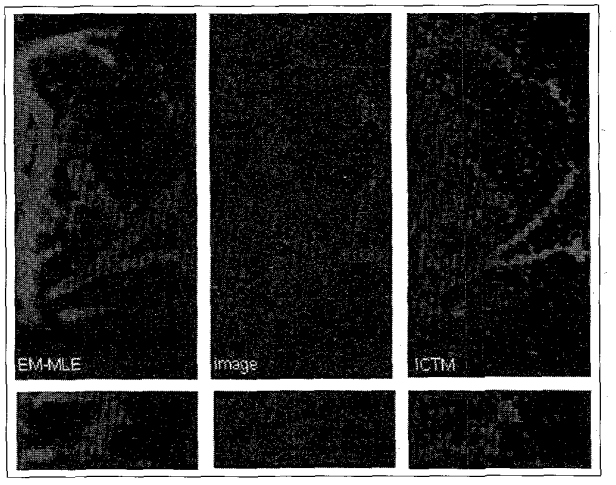

12. Mouse 3T3 fibroblast stained for tubulin. The confocal image is shown in the middle images, the EM-MLE result on the left, and ICTM result on the right. An x-y slice (top) and and an x-z slice (bottom) are shown for all 3-D images.

To quantify this improvement with a single value, Van der Voort and Strasters [2] summed all voxel values in the GDT transformed image. We used the same procedure to compare the improvement of EM-MLE and ICTM restoration for this specific kind of texture analysis. In contrast to their simulation experiments, we generated images with multiple cylindrical objects (Fig. 8) with noise to simulate a more a "realistic" confocal image. The GDT sum values of the confocal image of the generated cylinders, as well as the values of the EM-MLE and ICTM results, are shown in Fig. 9. This figure shows a considerable reduction of the GDT sum value for ICTM. The reduction of the EM-MLE reconstructed images is an order of magnitude better than the ICTM results. However, the % error of the EM-MLE GDT values are negative in most cases, indicating a smaller GDT value for the EM-MLE result compared to object GDT value. The result of the EM-MLE and ICTM restoration of the cylindrical objects are shown in Fig. 10, their GDT images are shown in Fig. 11.

Restoration of Confocal Images: Mouse 3T3 Fibroblast Stained for Tubulin

A specimen was prepared of Mouse 3T3 fibroblast stained for tubulin. Anti-Tubulin, rat IgG monoclonal antibody at a 1:100 dilution, (Sera-lab) was used as primary anti-body. For a secondary antibody, polyclonal Donkey-anti-Rat, IgGs-FITC labeled [21], was used at again a 1:100 dilution. Fixation and immunocytochemical staining conditions are as described by Wansink, et al. [22].

The confocal images were recorded with an Aristoplan Leica (model 0001) confocal microscope, series 1000, with a 100x oil immersion objective, with a NA of 1.32. The image size is 512 x 512 x 32 pixels at zoom 2 with a Z-step 0.208 μm, giving a field size of 25 x 25 x 6 μm. The voxel size is 49 x 49 x 208 nm, slightly above the Nyquist criterion. To measure the CPSF (see above), about 10 green fluorescent micro-beads (diameter 49 nm, Polysciences) were recorded using the same CFM setup as is used for the regular images.

The diameter of a microtubule is 25 nm, the primary and secondary antibodies add about 24 nm. Therefore the diameter of a single, stained tubule adds up to 49 nm, about the size of lateral sampling distance. Figure 12 shows the confocal image of the tubulin and the restoration results of the EM-MLE and ICTM algorithm. Both results were obtained using the Huygens [23] system running on a SGI Power Indigo2 computer (Silicon Graphics, Mountain View, CA 94043).

Conclusions

We have compared the performance of the EM-MLE and ICTM restorations applied to confocal images. Both methods greatly reduce diffraction-induced distortions of confocal images. Due to their non-linearity, both are able (partially) to restore data of missing frequencies. From our experiments, it is clear that for our test objects, the EM-MLE algorithm performs much better than ICTM. The EM-MLE algorithm produces better results under all the conditions we tested, and with respect to all three performance measures (I-Divergence, MSE, GDT) we used. Only for high SNR conditions, the MSE performance of ICTM approaches the EM-MLE results. It must be noted that this conclusion is only valid for the type of objects we used in our experiments (sparse objects); it may well be that for more dense objects, the situation is different. The poor ICTM performance shows that its functional is not well suited for images distorted with Poisson noise.

We did not find artifacts such as ringing in the results of either algorithm. The restoration results on the cylindrical objects show, however, that the EM-MLE algorithm has a tendency to reconstruct an image that is sharper and smaller than the original object (Fig. 10). This aspect of EM-MLE should be investigated thoroughly. Greander's method of Sieves [9] seems promising for regularizing the EM-MLE algorithm.

Finally, to reduce the computational burden of ICTM and EM-MLE (Fig. 3), methods to speed up these algorithms should be investigated more fully [3].

Acknowledgements

We are grateful to Professor I.T. Young and Dr. L.J. van Vliet for their thorough reading of the draft version of this article. We thank Marlies Buijs for her help with the specimem preparations.

References

1. **Wijnaends van Resandt RW, Marsman HJB, Kaplan R, Davoust J, Stelzer EKH, Stricker R:** Optical fluorescence microscopy in 3 dimensions: microtomoscopy. *J. of Microscopy* 138: 29-34, 1985.

2. **Van der Voort HTM, Strasters KC:** Restoration of confocal images for quantitative image analysis. *J of Microscopy* 178 (2): 165-181, 1995.

3. **Snyder DL, Hammoud AM, White RL:** Image recovery from data acquired with a charge-coupled-device camera. *J of the Optical Society of America* 10 (5): 1014-1023, 1993.

4. **Holmes TJ, Bhattacharyya S, Cooper JA, Hanzel D, Krishnamurti V, et al:** Light Microscopic Images reconstructed by maximum likeli-

hood deconvolution. *Handbook of biological Confocal Microscopy,* Plenum Press, New York, pp 389-402, 1995.

5. **Grochmalicki J, Pike ER, Walker JG, Bertero M, Boccacci P, Davies RE:** Superresolving masks for incoherent scanning microscopy. *J of the Optical Society of America* 10 (5): 1074-1077, 1993.

6. **Carrington WA, Lynch RM, Moore ED, Isenberg G, Fogarty KE, Fay FS:** Superresolution Three-Dimensional Images of Fluorescence in Cells with Minimal light exposure. *Science* 268: 1483-1487, 1995.

7. **Shaw PJ, Rawlins DJ:** The point-spread function of a confocal microscope: its measurement and use in deconvolution of 3-D data. *J of Microscopy* 163 (2): 151-166, 1991.

8. **Hanninen PE, Hell SW et al:** Two photon excitation 4π confocal microscope: enhanced axial resolution microscope for biological research. *Applied Physics Letters* 66(13): 1698-1701, 1995.

9. **Snyder DL, Miller MI:** *Random Point Processes in Time and Space,* 2nd Edition, Springer-Verlag, New York, 1991.

10. **Dempster AP, Laird NM, Rubin DB:** Maximum Likelihood from Incomplete Data via the EM Algorithm. *J of the Royal Statistical Society* B 39: 1-37, 1977.

11. **Shepp LA, Vardi Y:** Maximum Likelihood Reconstruction for Emission Tomography. *IEEE Trans on Medical Imaging* MI-1: 113-121, 1982.

12. **Vardi Y, Shepp LA, Kaufman L:** A Statistical Model for Positron Emission Tomography. *J Am Statistical Association* 80: 8-35, 1985.

13. **Richardson WH:** Bayesian-based iterative method of image restoration. *J of the Optical Society of America* 62: 55-59, 1972.

14. **Lagendijk RL:** Iterative identification and restoration of images, PhD thesis, Delft University of Technology, 1990.

15. **Press WH, Flannery BP, Teukolsky SA, Vetterling WT:** *Numerical Recipes in C,* University Press, Cambirdge UK, 1988.

16. **Holmes TJ, Li YH:** Acceleration of maximum-likelihood image restoration for fluorescence microscopy and other noncoherent imagery. *J of the Optical Society of America* 8 (6), 1991.

17. **Bracewell RN:** Discrete Hartley Transform. *J of the Optical Society of America* 73: 1832-1835, 1983.

18. **Van Vliet LJ:** *Grey-scale Measurements in multi-dimensional digitized Images,* PhD Thesis, Delft University Press, Delft, The Netherlands, 1993.

19. **Csiszar I:** Why Least Squares and maximum entropy? An axiomatic approach to inference for linear inverse problems. *The Annals of Statistics* 19 (4): 2032-2066, 1991.

20. **Snyder DL, Schutz TJ, O'Sullivan JA:** Deblurring subject to Nonegative Constraints. *IEEE Trans on Signal Processing* 40, pp 1143-1150, 1992.

21. **712-096-150:** Jackson Immuno Research Laboratories Inc., West Grove, Pennsylvania, USA.

22. **Wansink DG et al:** RNA polymerase II transcripts is concentrated outside replication domains throughout S-phase. *J of Cell Sci.* 107: 1449-1456, 1994.

23. **Scientific Volume Imaging B.V.:** J. Geradtsweg 181, 1222 PS Hilversum, The Netherlands.

Geert M.P. van Kempen received his Masters degree in applied physics on September 1993, at the Delft University of Technology, the Netherlands. His Masters thesis is titled Restoration of Scanning Tunneling Microscope Images. Currently, he is a Ph.D. student at the Pattern Recognition Group of the Delft University of Technology. His main topics of interest are image restoration, fluorescence microscopy, quantitative measurement theory and color imaging. He can be reached at the Pattern Recognition Group, Delft Univeristy of Technology, Lorentzweg, 2628CJ Delft, The Netherlands.

Hans T.M. van der Voort studied physics at the University of Amsterdam. After receiving an MS in 1981, he became active in the field of confocal microscopy. His work included the design of image processing systems, theory of microscopic image formation, volume visualization and image restoration. He received his Ph.D. in 1989 with a thesis titled "Three Dimensional Image Formation and Processing in the Confocal Microscope+. His special interests lie in image restoration and interactive volume exploration. In 1994 he founded his own software company, Scientific Volume Imaging B.V.

Jan G.J. Bauman received his Masters degree in biology on march 1975, at the State University Leiden, the Netherlands. His mayor was biology with chemistry, other topics were Genetics and Histochemistry. He received his Ph.D. degree at the University of Leiden on 19 march 1980. His thesis is titled +Cytochemical detection of specific nucleic acid sequences. Development and application of in situ hybridization methods for fluorescence microscopy+. Currently, he is employed as a Post Doctoral fellow at the University of Amsterdam, the Netherlands at the E.C. Slater Institute, faculty of chemistry. His main topics of interest are now nuclear architecture as studied by multicolor histochemical techniques and confocal microscopy.

Karel C. Strasters received his MSc in electrical engineering in 1989 and his Ph.D. in applied physics in 1994 from the Delft University of Technology, the Netherlands. His thesis was titled "Quantitative Analysis in Confocal Image Cytometry" covering different aspects of confocal image restoration, image segmentation and texture and image analysis. Currently Dr. Strasters is employed by Philips Medical Systems where his primary research interests are three dimensional image processing, combining multiple medical imaging modalities, and image guided surgery.